PNAS RESEARCH ARTICLE | CHEMISTRY MEDICAL SCIENCES OPEN ACCESS

# Gluing blood into gel by electrostatic interaction using a water-soluble polymer as an embolic agent

Zhiping Jin[a], Hailong Fan[b,1], Toshiya Osanai[a,1], Takayuki Nonoyama[c], Takayuki Kurokawa[c], Hideki Hyodoh[d], Kotaro Matoba[d], Akiko Takeuchi[e], Jian Ping Gong[b,c], and Miki Fujimura[a]

Edited by Anna Balazs, University of Pittsburgh, Pittsburgh, PA; received April 18, 2022; accepted September 19, 2022

**Liquid embolic agents are widely used for the endovascular embolization of vascular conditions. However, embolization based on phase transition is limited by the adhesion of the microcatheter to the embolic agent, use of an organic solvent, unintentional catheter retention, and other complications. By mimicking thrombus formation, a water-soluble polymer that rapidly glues blood into a gel without triggering coagulation was developed. The polymer, which consists of cationic and aromatic residues with adjacent sequences, shows electrostatic adhesion with negatively charged blood substances in a physiological environment, while common polycations cannot. Aqueous polymer solutions are injectable through clinical microcatheters and needles. The formed blood gel neither adhered to the catheter nor blocked the port. Postoperative computed tomography imaging showed that the polymer can block the rat femoral artery in vivo and remain at the injection site without nontarget embolization. This study provides an alternative for the development of waterborne embolic agents.**

liquid embolic agent | electrostatic interaction | adjacent sequence

## Significance

Development of a water-soluble polycation that can glue negatively charged blood contents together but not trigger coagulation could be a new approach to realize the embolization. However, it is a significant challenge since electrostatic interaction normally diminishes in saline water due to the Debye screening effect. Here, we discovered that a polymer-bearing adjacent cationic/aromatic sequence can glue the blood components together, forming a blood gel through electrostatic interactions in the physiological environment, which common polycation cannot. The blood gel is soft, viscoelastic, stable, and shows nonadhesion to the microcatheter. In vivo experiments showed that the blood gel can fully occlude murine vasculature without fragmentation or nontarget embolization. This work provides a new idea for the realization of vascular embolization.

Endovascular embolization is a common treatment for cerebrovascular diseases such as cerebral arteriovenous malformations (cAVMs) and cerebral aneurysms. This therapy is based on the use of a variety of embolic agents to occlude one or more blood vessels or abnormal vessels using an intravascular microcatheter. Depending on the disease type and embolic material, endovascular treatment can be performed either alone or in combination with another method (1–4).

At present, the three main types of embolic materials include mechanical occlusion devices, particulates, and liquid embolic agents (LEAs) (5). These agents can also be subcategorized into temporary and permanent embolic materials based on their properties (6). Among them, LEAs are the most common material for cAVMs and dural arteriovenous fistula treatments, which are generally triggered by environmental changes between administration (e.g., syringe, catheter) and operating conditions (e.g., blood vessels). LEAs with low viscosities are required to pass through delivery systems and form solid-like materials after exiting. Solidification can be realized by polymerization, precipitation, or gelation (7–10). *N*-Butyl-2-cyanoacrylate (nBCA) (TruFill) is a typical polymerization-based liquid embolic agent. nBCA is a water-insoluble liquid monomer that can rapidly (in seconds) polymerize upon contact with an ionic substance ($OH^-$) in body fluid; however, fast polymerization may lead to nontarget embolization and adherence of the catheter to the vessel walls (11, 12). Precipitation-based LEAs (e.g., Onyx) are water-insoluble polymers dissolved in the organic solvent dimethyl sulfoxide (DMSO). When the liquid exits the catheter, DMSO rapidly diffuses into the blood, and the polymer precipitates. The use of organic solvents entails certain safety risks; for example, the rapid injection of DMSO solutions induces vasospasm and can cause neurotoxicity and vascular toxicity (11, 13). In contrast to the above systems, gelation-based LEAs are waterborne systems. Such water-soluble polymers usually contain functional groups that are sensitive to temperature, Ph, and/or ionic strength. Gelation-based embolic agents require a well-defined gelation time to block lesions while preventing catheter blockage and nontarget embolization (14–16).

Despite their excellent performance, all of these classical liquid embolic materials have certain shortcomings that limit the effectiveness of treatment, including neurotoxicity and angiotoxicity by using an organic solvent, adhesion of the microcatheter to the embolic agent, incomplete occlusion, and unintentional catheter retention (5, 9, 17). To the best of our knowledge, the clots formed by these LEAs undergo embolization based on their phase transition. In mammals, fibrin polymerization and platelet activation lead to a blood clot, which is mainly composed of aggregated blood contents (e.g., red blood cells [BCs]). These blood clots can act as hemostatic agents physiologically and pathologically obstruct arteries or veins (18). Based on this mechanism, a water-soluble

Competing interest statement: Z.J., H.F., T.O., T.N., and T.K. are inventors of a patent application (2022-030098) entitled "Embolic Agents and Vascular Embolization Kit" submitted by Hokkaido University, which covers the composition and application of poly(cation-π) materials.

This article is a PNAS Direct Submission.



[1]To whom correspondence may be addressed. Email: fanhl@icredd.hokudai.ac.jp or osanait@med.hokudai.ac.jp.

This article contains supporting information online at http://www.pnas.org/lookup/suppl/doi:10.1073/pnas.2206685119/-/DCSupplemental.

Published October 10, 2022.

polymer that can glue blood contents together but does not trigger coagulation can be developed as a strategy to achieve embolization while overcoming the above-mentioned shortcomings.

The main substances in human blood are BCs and proteins, whose surfaces are negatively charged (19). Therefore, the electrostatic interactions between cationic polyelectrolytes and blood substances can be used as an alternative route to achieve vascular embolization. However, the electrostatic interaction between oppositely charged surfaces normally diminishes in saline water owing to the Debye screening effect, which prevents the formation of a blood gel (20). Recently, inspired by the amino acid sequence of protein kinase C, our group synthesized a series of water-soluble polymers bearing adjacent cation-aromatic sequences named poly(cation-*adj*-π) (*adj* is short for adjacent and π for aromatic monomer) (21). Aromatics on copolymers were found to enhance the electrostatic interactions of their adjacent cationic residues with the counter surfaces, even in a high ionic-strength medium (22).

In this study, we discovered that poly(cation-*adj*-π) can glue blood components together, forming a blood gel through electrostatic interactions in the physiological environment, which common polycations cannot (Fig. 1). Blood gel is soft, viscoelastic, and stable. No obvious adhesions to the microcatheter were observed. The embolic process and effect of the blood gel glued by poly(cation-*adj*-π) were validated by in vitro and in vivo experiments. Although this work is still in the early stages of research, it provides an idea for the realization of vascular embolization and could serve as a different direction for the development of the next generation of waterborne embolic agents.

## Results and Discussion

**Formation of Blood Gel.** An adjacent cation-aromatic sequence polymer was synthesized by free-radical copolymerization of equimolar amounts of cationic and aromatic monomers in DMSO at 1.0 M concentration (Fig. 1*A*). The polymers were subsequently purified by dialysis and lyophilization, followed by dissolution in water at different concentrations and ultraviolet (UV) sterilization (21).

Different types of poly(cation-*adj*-π) were mixed with citrated blood collected from Sprague-Dawley rats to confirm whether poly(cation-*adj*-π) can interact with blood. Fig. 2*A* shows that poly(cation-*adj*-π) at different concentrations can rapidly interact with blood within 1 min to form a stable blood gel. By contrast, the cationic homopolymer poly 2-(acryloyloxy) ethyl trimethyl ammonium chloride) (P(ATAC)) cannot form a stable blood gel after washing with normal saline because the cationic group alone cannot form strong electrostatic interactions in saline water owing to the Debye screening effect (20). As a control, we added $CaCl_2$ to activate the coagulation. The results showed that a stable coagulum could not be formed in a short time.

To investigate the relationship between the amount of polymer and blood gel mass, poly(ATAC-*adj*-PEA) was selected as a representative. Different amounts of polymer solutions at different concentrations were added to citrated blood (0.5 mL), and the formed blood gel was weighed (Fig. 2*B*). The results showed that with an increase in the volume of the polymer solution, the mass of the blood gel increased and then plateaued with a similar mass. The plateau start point shifted to higher values with a decrease in polymer concentration, but the polymer mass at each point was similar. We further compared the mass of the blood gel formed by adding 150 μL of different poly(cation-*adj*-π) into citrated blood (0.5 mL). No obvious difference in blood gel mass was observed between polymers (Fig. 2*C*). These results indicate the existence of a saturation mass of the formed blood gel within a certain volume of blood that is not related to the amount of added polymer. This finding confirms that the blood gel is mainly composed of substances in the blood, while the poly(cation-*adj*-π) works as a glue to bind them together. Moreover, the proper injection volume can be calculated after preoperative assessment, which not only prevents the overuse of the polymer but also reduces the cost of treatment.

The mechanical properties of the blood gel were measured using a rheometer. Rheological results showed that the blood clot prepared by adding $CaCl_2$ to citrated blood had a frequency-independent storage modulus $G'$. This indicated that the blood clot possessed an elastic polymer network, which was consistent with the notion that clots are composed of a three-dimensional (3D) network of fibrin fibers (23). By contrast, the blood gel formed by poly(ATAC-*adj*-PEA) exhibited viscoelastic behavior and a strong frequency dependence of $G'$, which is larger than the loss modulus $G''$ over the tested frequency range; this indicated that the blood gel was a solid-like gel (Fig. 2*D*). After prolonged soaking in normal saline water, the blood gel became contracted and squeezed out the fluid contents, leading to an increase in modulus ($G'$ and $G''$) compared with those of the as-prepared state. These results implied the stability of the blood gel and supported further investigation into the potential of poly (cation-*adj*-π) as an embolic agent.

Considering the multiple substances in the blood, citrated rat blood was centrifuged to obtain platelet-poor plasma (PPP) and BCs (mainly red BCs) (24). Then, the obtained contents were mixed with poly(ATAC-*adj*-PEA) solutions, and both PPP and BC formed a stable agglomerate with poly(ATAC-*adj*-PEA) (Fig. 2*E*). Histological photomicrographs (hematoxylin and eosin [H&E] staining) confirmed the absence of an obvious network structure in eosin-stained red BC agglomerates (*SI Appendix*, Fig. S1), thereby indicating that poly(ATAC-*adj*-PEA) solutions can glue BCs to form a blood gel.

In mammalian blood, fibrinogen and prothrombin are the two main plasma proteins that are closely related to coagulation, a process that entails a complicated cascade of enzyme activation events (18). Usually, fibrinogen is enzymatically converted to fibrin by thrombin, forming a fibrin-based blood clot. Thrombin is produced by the enzymatic cleavage of prothrombin through activated factor X and its cofactor (factor V) in conjunction with calcium (18). In our study, the anticoagulant citrate dextrose solution (ACD-A) was added to the blood for anticoagulation. Citrate interrupts the blood clotting process by forming a calcium citrate complex, which disrupts the conversion of prothrombin to thrombin (25). Therefore, we believe that the formation of "white clot" is based mainly on the electrostatic interactions between poly(cation-*adj*-π) and negatively charged plasma proteins in PPP, while the "red clot" was formed by the electrostatic interactions between poly(cation-*adj*-π) and negatively charged red BCs.

**In Vitro Injectability Test.** No significant difference was observed between each polymer in the formation of the blood gel; therefore, poly(ATAC-*adj*-PEA) was selected as a representative for the subsequent in vitro and in vivo experiments to check the potential application of poly(cation-*adj*-π) as a liquid embolic agent.

To confirm injectability, we replicated the injection process by injecting a polymer solution through clinical needles and catheters. The injection force was recorded using a mechanical

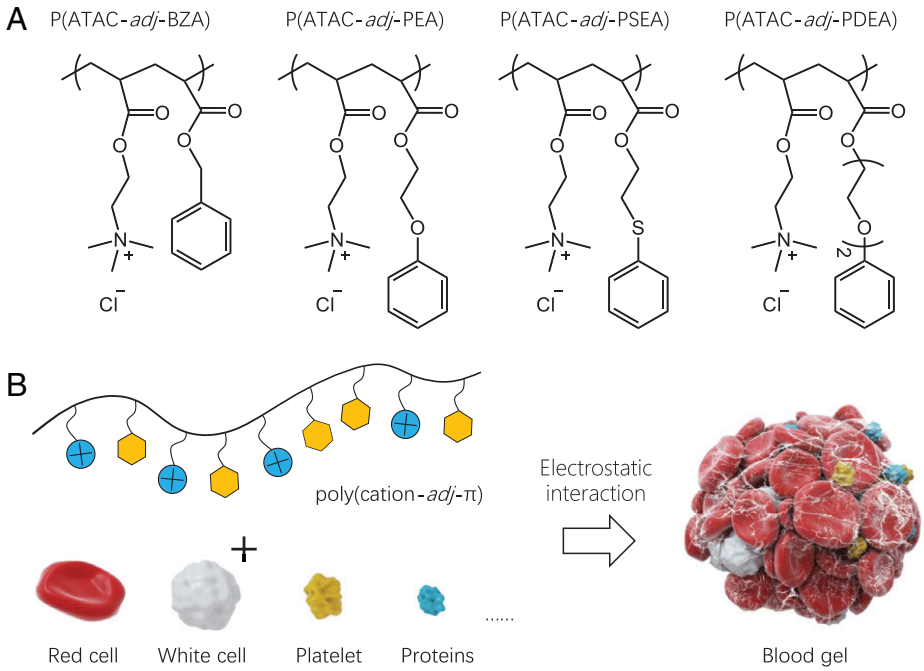


**Fig. 1.** Schematic illustration of blood gel formation strategy. (*A*) Chemical structures of poly(cation-*adj*-π). (*B*) Schematic illustration of poly(cation-*adj*-π) glued the negatively charged blood substances into a blood gel.

tester (Fig. 3*A*). We measured the injection force of the polymer solution using 32G clinical needles (inner diameter[I.D.] 0.26 mm), as shown in Fig. 3 *A*, *a*. The results showed that poly(ATAC-*adj*-PEA) can be smoothly injected through needles. Polymer concentration and injection rate significantly affected the injection force, which first increased and then plateaued in all of the tests (Fig. 3 *B*–*D*). A high polymer concentration leads to a high solution viscosity, resulting in a large injection force. Meanwhile, high injection rates require a high injection force, which agrees with Poiseuille's law for fluid flow in tubes (26).

To further verify the injectability of the polymer in clinical treatment, the polymer solution was mixed with a contrast agent (tantalum powders, 0.25 g/mL, *SI Appendix*, Fig. S2), and the injection force of mixtures through clinical microcatheters (I.D. 0.43 mm, length 150 cm), whose port was immersed in the citrated blood bath, was measured (Fig. 3 *A*, *b*). To imitate the discontinuous injection during real operation, the program was set to continue the injection for 7 s and then pause for 3 s, and then run for a total of 4 times. For the poly(ATAC-*adj*-PEA) solution, the force increased to approximately 10 N during injection and decreased during the pause in each cycle. No obvious change in the force curve of each cycle was observed, indicating that the port was not blocked by the blood gel. For comparison, the same process was used to test the clinical embolic agent Onyx 18. The injection force of Onyx 18 continually increased after each pause, indicating that the precipitated polymers partially blocked the microcatheter port.

In clinical applications, injection force is an important parameter for LEAs, which not only determines the suitability of the agent for clinical use but is also related to embolization treatment (physician administration and treatment effect) (27). The injection force can be affected by many factors, including the properties of the liquid agent (e.g., concentration, viscosity), injection rate, type of syringe and microcatheter, and injection conditions (e.g., air, liquid, tissue) (28, 29). Injection force should be sufficiently low to be usable by physicians. According to a review paper by Hu et al., the maximum forces of a typical injection applied by a male and a female are approximately 95.4 and approximately 64.1 N, respectively (5). Therefore, each polymer concentration tested in this study required comfortable forces between 4 and 10 N, which meets the basic requirements for a liquid embolic agent.

**Adhesiveness between Embolic Agents and the Catheter.** Preventing the adhesion of the catheter to embolic agents is another important factor for evaluating embolic agents. Although Onyx is recognized as a nonadhesive embolic agent, clots easily form around the microcatheter, thereby increasing the risk of hemorrhage during extraction (16, 30, 31). To confirm this finding, an in vitro traction test was conducted. As shown in Fig. 4*A*, a thin polyethylene tube (I.D. 0.28 mm) was inserted into a thick polyethylene tube (I.D. 1.4 mm) filled with 0.5 mL citrated rat blood, and the same volume of poly(ATAC-*adj*-PEA) solution was injected into the middle part of the blood through a thin polyethylene tube. After standing for 30 min, the thin polyethylene tube was withdrawn, and the force used during the pulling process was simultaneously recorded. Fig. 4 *B* and *C* show that the traction force of the poly(ATAC-*adj*-PEA)-based blood gel was much lower than that of Onyx 18 and similar to that of nonagglomerate samples using normal saline. The results indicated that the blood gel formed by poly(ATAC-*adj*-PEA) showed no obvious adhesion to plastic tubes, thereby considerably reducing the risk of hemorrhage in the traction process.

**Biocompatibility of Poly(cation-*adj*-π).** To confirm the biocompatibility of poly(cation-*adj*-π) and enable easy observation, a polymer solution and a poorly flowing entangled polymer hydrogel were used to conduct the experiment. In the experimental group, 50 μL of 40 mg/mL poly(ATAC-*adj*-PEA) aqueous solution and a disk-shaped (Ø 5 mm, thickness 1 mm) poly(ATAC-*adj*-PEA) gel were implanted under the dorsal skin for 7 and 28 d, respectively, and rats with skin incision only were used as sham controls (Fig. 5*A*). Clinical serum biochemical tests and histological analyses of skin tissues were performed for

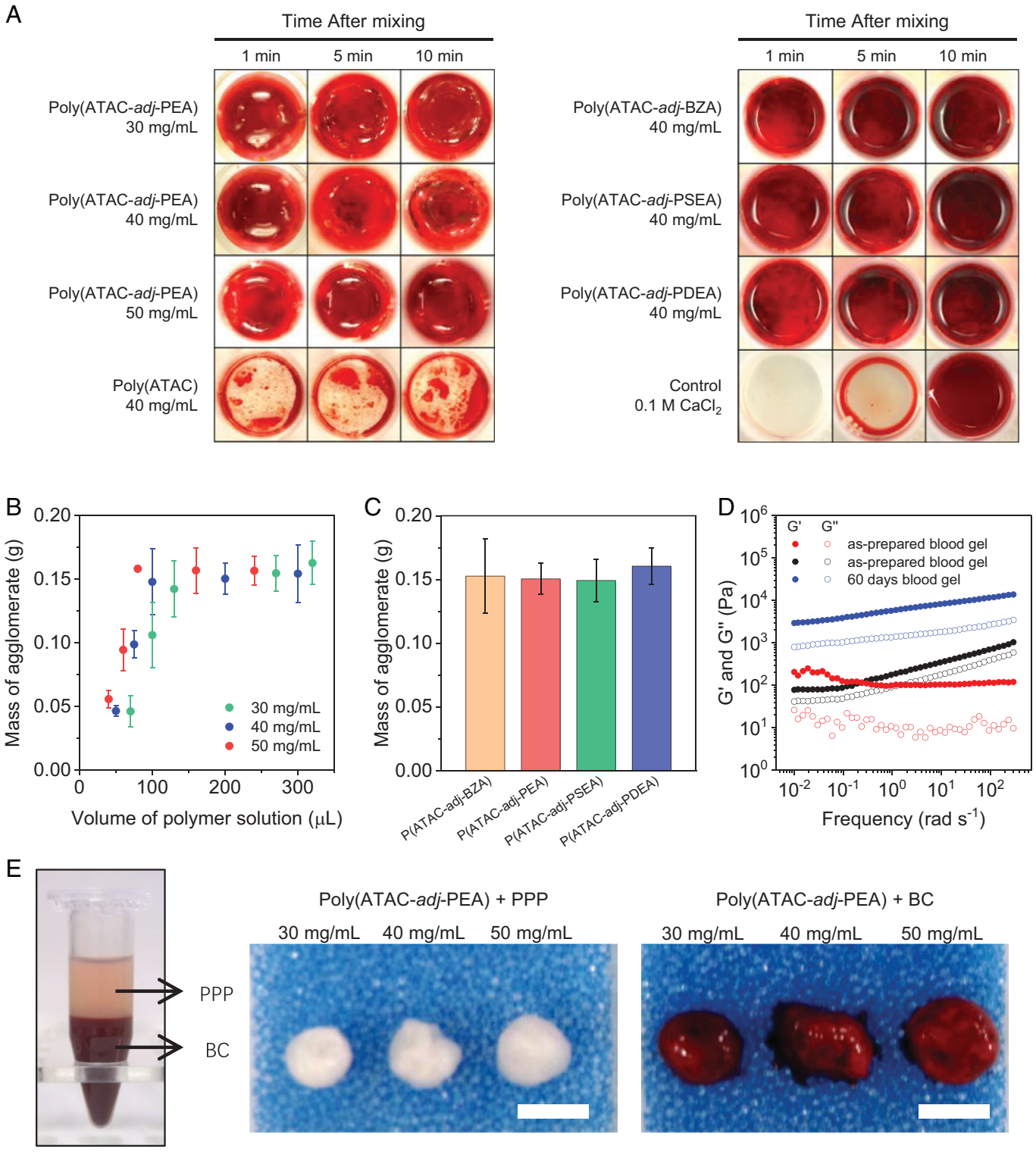


**Fig. 2.** In vitro formation of blood gel. (*A*) Blood gel formation as a function of time and polymers. (*B*) Weight of blood gel formed by mixing 0.5 mL citrated blood with different amounts of poly(ATAC-*adj*-PEA) solutions. (*C*) Weight of blood gel formed by mixing 0.5 mL citrated blood with 150 μL of 40 mg/mL poly(cation-*adj*-π) solutions. (*D*) Rheological behaviors of blood gel at the as-prepared state and after soaking in normal saline for 60 d. Blood gel formed by mixing 1.0 mL citrated blood with 1.0 mL of 40 mg/mL poly(ATAC-*adj*-PEA) solutions. (*E*) Digital picture of blood gel by mixing 200 μL of 40 mg/mL poly(ATAC-*adj*-PEA) with 200 μL PPP and BCs, respectively. Scale bars, 0.5 cm.

comparison. In this study, alanine aminotransferase and aspartate aminotransferase were used to assess liver function after polymer or hydrogel plantation, whereas creatinine and blood urea nitrogen were used to assess renal function. Then, H&E staining and immunostaining (CD3, Abcam, UK) were simultaneously conducted to confirm whether severe inflammatory response occurred after implantation. After surgery, all of the rats were in good health, and no swelling or redness was observed on the skin around the incision (*SI Appendix*, Fig. S3). As shown in Fig. 5 *B* and *C*, compared to those of rats in the sham group, the four parameters did not increase in tested rats within 4 wk after gel and polymer solution implantation.

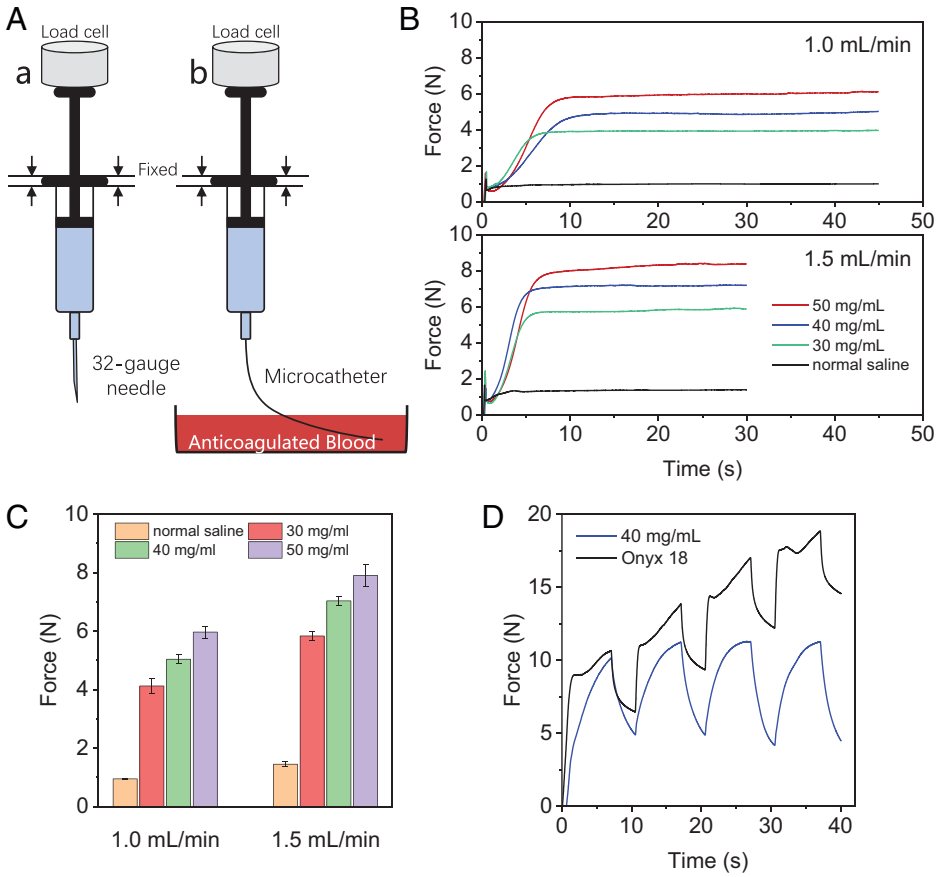


**Fig. 3.** In vitro injectability of poly(cation-*adj*-π). (*A*) Schematic illustration of injection force test by using a 1-mL syringe with (*a*) 32G needle and (*b*) microcatheter. (*B*) Injection force curves of poly(ATAC-*adj*-PEA) and normal saline solution through a 32G needle under different injection rates. (*C*) Injection force values at the plateau region of poly(ATAC-*adj*-PEA) and normal saline solution through a 32G needle. The error bars indicate SD ($n$ = 3). (*D*) Injection force curves of poly(ATAC-*adj*-PEA) and Onyx 18 through a 150-cm-long microcatheter with 1.0 mL/min injection rate. The program was set to continue the injection for 7 s and then stop for 3 s and be repeated 4 times.

H&E staining and immunostaining results also showed no obvious inflammation around the incision in either the polymer or hydrogel groups, demonstrating the safety and low toxicity of the poly(ATAC-*adj*-PEA) aqueous solution and hydrogel in rats (Fig. 5*D* and *SI Appendix*, Fig. S4). In addition, we implanted the poly(ATAC-*adj*-PEA) hydrogel under the dorsal skin to evaluate its stability in the body. On the 50th day after surgery, the hydrogels were taken out. The hydrogel volumes shrank, but the shapes did not change (*SI Appendix*, Fig. S5), which may arise from the decrease in gel osmotic pressure by absorbing the negatively charged small molecules from the tissue fluid. The results indicate good stability of the polymers in the body.

**In Vivo Embolization in Rat Femoral Artery.** To assess the possibility of in vivo nontarget embolization of the poly(cation-*adj*-π) aqueous solution, 0.1 mL of 40 mg/mL poly(ATAC-*adj*-PEA)

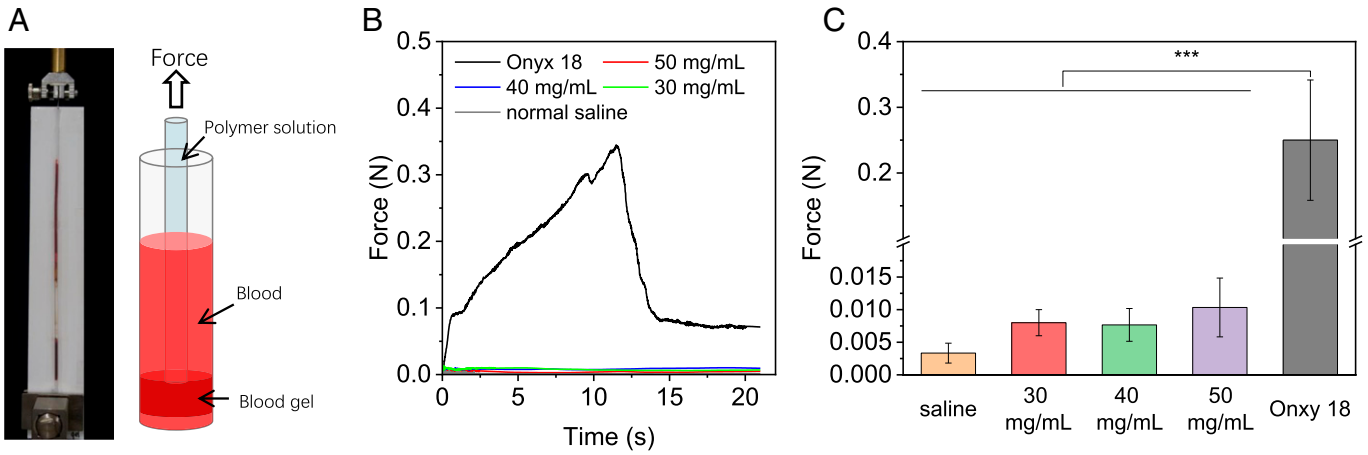


**Fig. 4.** Adhesiveness of embolic agents to polyethylene tube. (*A*) Digital photograph and scheme illustration of traction force measurement. (*B*) Traction force curves of polyethylene tube pulling out of the blood after the blood gel was formed by poly(ATAC-*adj*-PEA) and Onyx 18. (*C*) The maximum force values during traction. The error bars indicate SD ($n$ = 3 in each group); ***$P$ < 0.001.

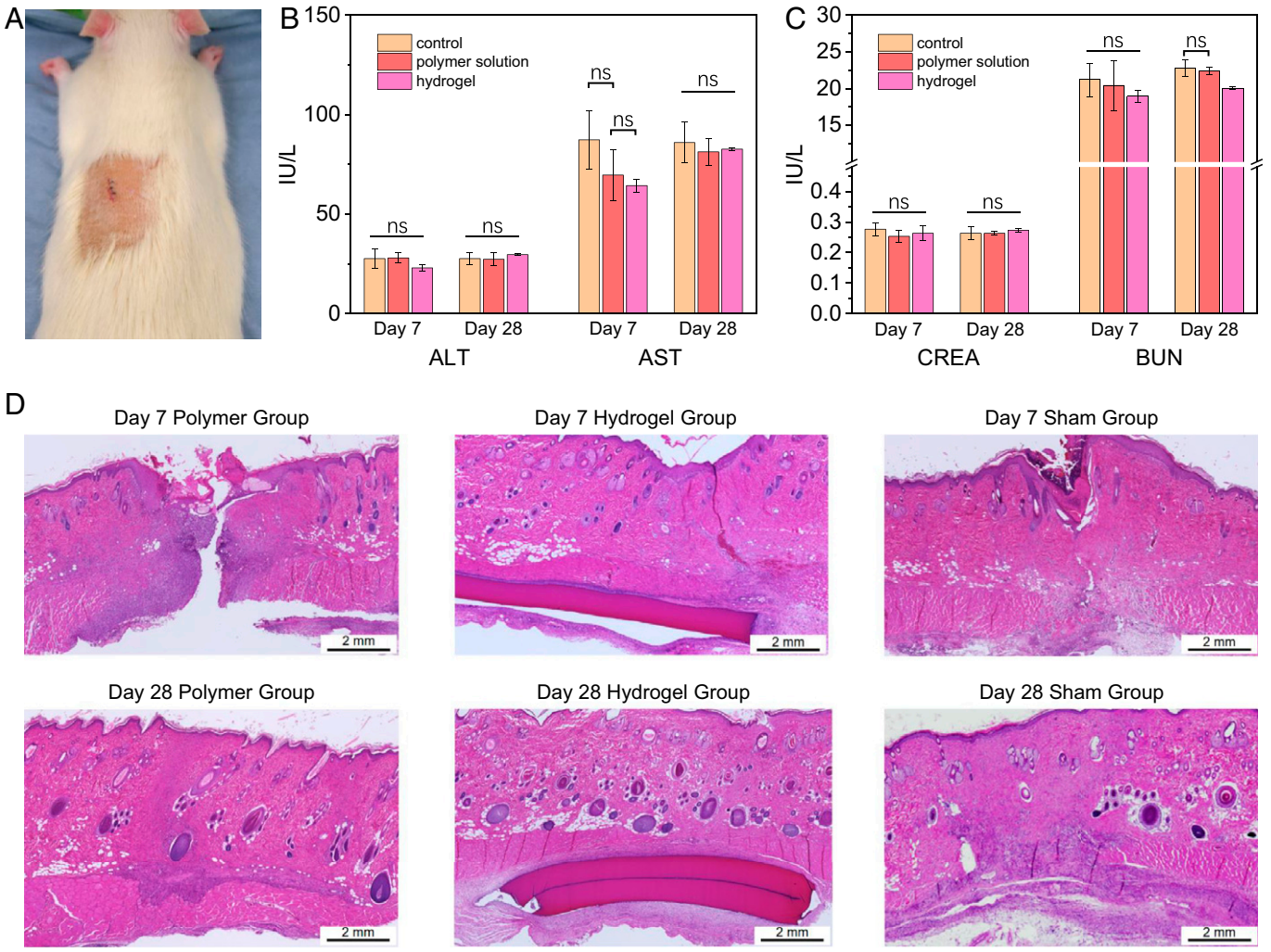


**Fig. 5.** Biocompatibility of poly(cation-*adj*-π). (*A*) Digital photograph of subcutaneous implantation (dorsal surgery incision) in rats. (*B*) Serum biochemical tests of liver function of rats at 7 and 28 d after implantation. (*C*) Serum biochemical tests of kidney function of rats at 7 and 28 d after implantation. (*D*) Histological photomicrographs (H&E staining) of the subcutaneous inflammatory response at 7 and 28 d after implantation. Data are shown as means ± SDs; ns, $P > 0.05$.

solution was injected into the right femoral artery of rats to form an embolism (Fig. 6*A*). After surgery, the right hindlimb with embolization gradually darkened and became unable to move, eventually leading to necrosis (Fig. 6*B*). Furthermore, H&E staining clearly showed occlusion clots left in vessels throughout the whole femoral artery and the branches. Red BCs and nuclei of white cells were observed, implying that the clot was formed by the aggregation of blood contents.

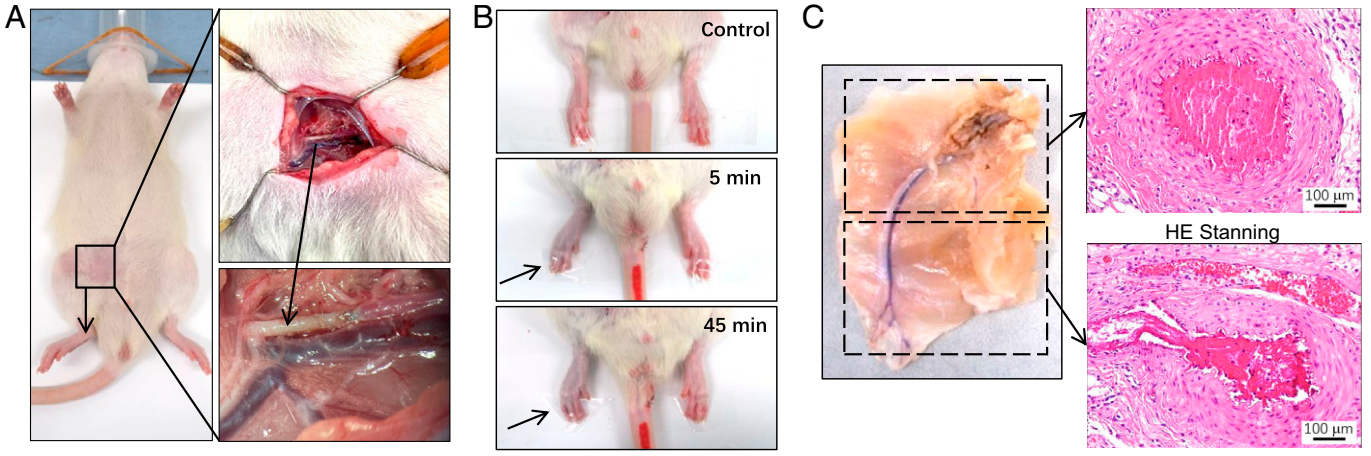


**Fig. 6.** In vivo embolization test. (*A*) Digital photographs of surgery area and rat's femoral artery after injection of poly(ATAC-*adj*-PEA) solution through a 32G needle. The *Left Arrow* indicates the distal injection, and the *Right Arrow* indicates the injection location. (*B*) Digital photographs of skin color change on rat's right hindlimb after surgery. (*C*) Histological photomicrographs of the right hindlimb with embolization.

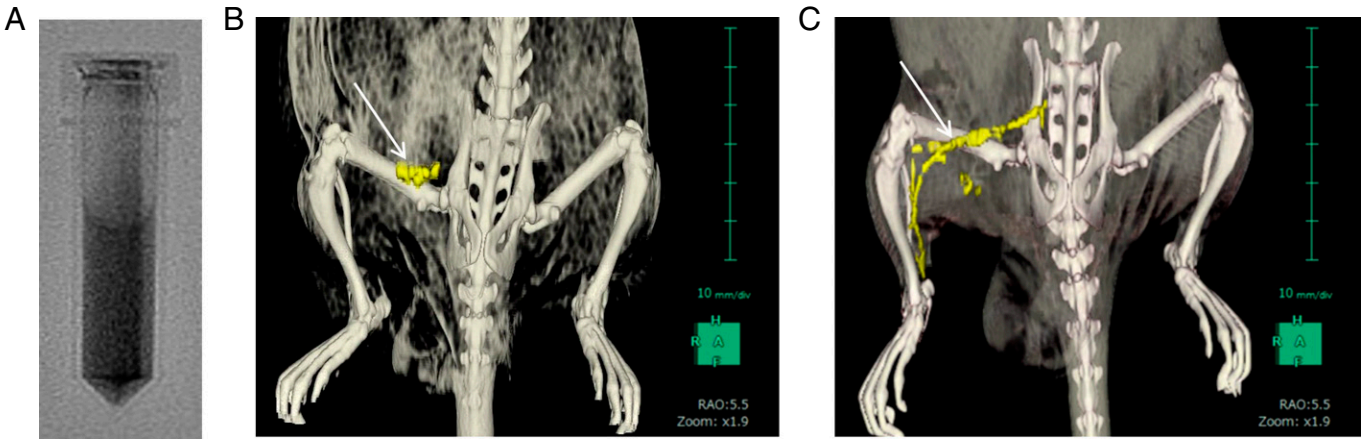


**Fig. 7.** In vivo postsurgery CT imaging. (*A*) X-ray image of 40 mg/mL poly(ATAC-*adj*-PEA) aqueous solution containing tantalum powders (0.25 g/mL) after 5 min of vibration. (*B*) CT image of rat after injection of 2 to 3 L poly(ATAC-*adj*-PEA) aqueous solution. (*C*) CT image of rats after injection of 0.05 mL poly(cation-*adj*-π) aqueous solution. Arrows indicate the radiopaque polymer, which is artificially colored yellow.

To further confirm the postradiopacity of poly(cation-*adj*-π), 40 mg/mL poly(ATAC-*adj*-PEA) solution containing tantalum powders (0.25 g/mL) was prepared for the experiment (Fig. 7*A*).Then, the mixture was injected in a single shot (2 to 3 μL) in the right femoral artery of rats, and computed tomography (CT) scanning was conducted at 3 h after injection. The CT results of the one-shot injection (Fig. 7*B* and *SI Appendix*, Fig. S6*A*) indicated that embolization only occurred near the injection site instead of flowing far forward with the blood. Then, 0.05 mL of the mixture was further injected into the rats' right femoral artery, which was subsequently CT scanned at 45 min after injection. The CT results (Fig. 7*B* and *SI Appendix*, Fig. S6*B*) showed that the mixture had good fluidity and could completely occlude the arteries of the right hindlimb; these findings were in agreement with the H&E staining results mentioned above. These results indicate that embolization based on gluing blood substances can be controlled by adjusting the injection volume and injection speed of poly(cation-*adj*-π) solution. This approach met the requirements for further targeted treatment with the aid of X-rays.

To verify the reproducibility of this approach, we have repeated the rat femoral artery injection experiment by using 10 rats (20 hindlimbs in total), 10 hindlimbs of which were injected with P(ATAC-*adj*-PEA) aqueous solutions (40 mg/mL, approximately 10 μL), and another 10 hindlimbs were injected with normal saline water (approximately 10 μL) as a control. After injecting the polymer solutions, the skin of the hindlimbs became dark and the tissue became necrotic over time (*SI Appendix*, Figs. S7 and S8). On the seventh day after injection, all of the rats were sacrificed and underwent CT scanning of hindlimbs. The CT 3D reconstruction images confirmed that all of the femoral arteries in the experimental group were occluded by the blood gels. In contrast, the hindlimbs injected with saline were healthy.

## Conclusions

In summary, we have demonstrated a conceptual strategy for endovascular embolization. In contrast to existing LEAs, whose embolization is based on the solidification of exotic materials, the water-soluble polymers bearing adjacent cation-aromatic sequences can glue negatively charged blood substances into a gel-like material through electrostatic interactions in normal saline water, whereas common polycations cannot form these interactions. Owing to its easy delivery through a microcatheter with low injection force coupled with biocompatibility and controlled embolization, the poly(cation-*adj*-π) aqueous solution is a promising liquid embolic agent. Further studies using in vivo models, such as cAVMs, arterial aneurysms, and cerebral tumors, will be conducted.

## Materials and Methods

**Materials.** ATAC (79.4% in water) was provided by Toagosei (Japan). 2-(Phenylsulfanyl)ethyl acrylate (PSEA), 2-(2-phenoxyethoxy)ethyl acrylate (PDEA), benzyl acrylate (BZA), and 2-phenoxyethyl acrylate (PEA) were provided by Osaka Organic Chemical (Japan). α-Ketoglutaric acid (UV initiator), DMSO, and tantalum powder were purchased from Wako Pure Chemical Industries (Japan). All of the chemicals were used as purchased without further purification. Millipore deionized water was used in all of the experiments.

**Synthesis of Poly(cation-*adj*-π).** The cationic monomer (0.5 M), aromatic monomer (0.5 M), and UV initiator (2-oxoglutaric acid, 0.25 mM) were first dissolved in DMSO; then, the mixture was polymerized under UV light irradiation (3.9 mW/cm$^2$, 11 h) in a glove box. Subsequently, the solution was loaded into a dialysis bag (cutoff molecular weight: 3,500), which was subsequently dipped in a large amount of water to remove DMSO and unreacted chemicals. The water was exchanged every 12 h for 1 wk. Following freeze-drying, pure poly(cation-*adj*-π) was obtained.

**Synthesis of Poly(cation).** The cationic monomer ATAC (1.0 M) and UV initiator (2-oxoglutaric acid, 0.25 mM) were first dissolved in water, and then the mixture was polymerized under UV light irradiation (3.9 mW/cm$^2$, 11 h) in a glove box. Subsequently, the solution was loaded into a dialysis bag (cutoff MW: 3,500), and the bag was dipped in a large amount of water to remove unreacted chemicals. Water was exchanged every 12 h for 1 wk. Following freeze-drying, pure poly(cation) was obtained.

**In Vitro Test.** All of the blood samples were extracted from 8-wk-old Sprague-Dawley rats (300 to 340 g) purchased from CLEA Japan and stored in ACD-A liquid purchased from Terumo Corporation Japan for anticoagulation.

PPP and BCs were obtained by centrifugation of whole blood as previously described (32). Briefly, 9 mL of whole blood was centrifuged (S700FR; Kubota Corporation, Japan) at 160 × *g* for 20 min to separate plasma from BCs. Then, the supernatant was pipetted at 4 mm below the dividing line between phases and transferred to a new tube. The remaining BCs were transferred to new tubes for further experiments. The second centrifugation for 15 min at 400 × *g* was performed on the previously obtained supernatants to separate the platelets to the maximum extent. The supernatants of the second centrifugation were used as PPP for further experiments.

A qualitative aggregation test was performed based on previous studies (27, 32). Briefly, 150 μL of polymer solutions at different concentrations were added to sequential wells of a 48-well plate, ensuring that the entire bottom

surface was coated with polymer. The same volume of citrated blood was then added to each well. At selected time points, normal saline was added to the wells to halt the reaction and aspirated immediately. The well was washed repeatedly until the solution became clear, which indicated the removal of all unaggregated blood components. Citrated blood (150 μL) with calcium chloride ($CaCl_2$, 0.1 M) at a volume ratio of 9:1 was used as a control.

A quantitative aggregation test was performed by weighing the mass of the blood gel. First, 500 μL of citrated blood was added to the microcentrifuge tubes. Second, different volumes of poly(cation-*adj*-π) aqueous solutions at different concentrations were slowly added to the blood. After injection, the blood gel was removed immediately and wiped with Kimwipes to remove surface liquid. Subsequently, the weight of the blood gel was measured by using a microbalance.

Rheological tests were performed using an ARES-G2 rheometer (TA Instruments, USA). A rheological angular frequency sweep from 0.01 rad $s^{-1}$ to 300 rad $s^{-1}$ was performed with a shear strain of 0.1% in the parallel-plate geometry at 37 °C. Disk-shaped samples with thicknesses of approximately 0.4 mm and diameters of 25 mm were placed on the plates and surrounded by normal saline solution.

An injection force test (14) using a 1-mL plastic syringe (Nipro Corporation, Japan) was performed on a Shimadzu tester (Autograph AG-X) using the Trapezium X software. The syringe was fixed to the tester to prevent it from moving during testing. The syringe plunger was depressed by a compression plate connected to a 100-N load cell to achieve injection at rates of 1 and 1.5 mL/min. For the needle injection test, poly(cation-*adj*-π) aqueous solutions with different concentrations were added to the syringe (Nipro Corporation, Japan) and injected through a 32G needle (Handaya, Japan). For the microcatheter injection test, a polymer solution (40 mg/mL) containing tantalum powders (0.25 mg/mL) was added to the syringe and injected through a 150-cm-long microcatheter (MSV150, Tokai Medical Products, Japan), the end of which was placed in a vessel containing anticoagulant blood. Onyx and normal saline were used as the references.

The traction force test was performed on a Shimadzu tester (Autograph AG-X) using the Trapezium X software. A thin polyethylene tube (I.D. 0.28 mm, outer diameter [O.D.] 0.61 mm) filled with each sample was inserted into a thick polyethylene tube (I.D. 1.4 mm, O.D. 1.9 mm) containing 0.1 mL citrated blood, and the same amount of polymer solution was injected into the blood. After standing for 30 min, the thin polyethylene tube was withdrawn at a rate of 100 mm/min. The force exerted during the pulling process was measured.

**In Vivo Test.** Eight-week-old Sprague-Dawley rats (300 to 340 g) were purchased from CLEA Japan and allowed free access to food and water. All of the animal experiments were approved by the Animal Study Ethical Committee of Hokkaido University Graduate School of Medicine.

Subcutaneous implantation for biocompatibility testing ($n = 18$) (32): A 1-cm skin incision was made on the right dorsal side of the rat. A small subcutaneous pocket was then created by blunt preparation. For the experimental group, 50 μL of 40 mg/mL poly(ATAC-*adj*-PEA) aqueous solution and a disk-shaped (Ø 5 mm, thickness 1 mm) poly(ATAC-*adj*-PEA) gel were embedded into the subcutaneous pocket. Then, the incision was anatomically closed, and the rat was allowed to recover from anesthesia. Rats with only a surgical incision were used as sham controls. At a selected time after surgery, blood (serum part) was collected for biochemical tests (SRL, Japan), and postperfusion tissues around the incision were collected for histological analyses (H&E staining, immunohistochemical staining, anti-CD3 antibody).

In vivo embolization ($n = 6$): A 1-cm incision was made longitudinally on the anterior thigh of the rat's right hindlimb. The femoral artery was exposed through a combination of sharp and blunt dissection under a surgical microscope. Two 7.0 silks (Akiyama Medical, Japan) were passed underneath the artery to allow for gentle manipulation of the artery by lifting and aligning the vessel for injection. Then, 0.1 mL poly(cation-*adj*-π) solution was injected distally into the artery using a 32G needle (Handaya). The incision was then closed anatomically, and the rats were allowed to recover from anesthesia. At 5 and 45 min after surgery, the hindlimb skin color was observed and recorded. Finally, all of the rats were anesthetized and perfused with saline at 4 °C, and the right hindlimb was subjected to histological analysis (H&E staining).

In vivo postsurgery CT imaging ($n = 6$): Poly(cation-*adj*-π) solution (40 mg/mL) containing tantalum powders (0.25 g/mL) was prepared before surgery. Different injection doses were used in the present study. In the first test, approximately 0.1 mL of the mixture was quickly injected into the right femoral artery of rats in the same procedure as the embolization test. After 45 min, the rats were subjected to CT scanning of the right hindlimbs to confirm embolization. The second test was a one-shot injection (2 to 3 μL) of the mixture into the rat's femoral artery using the same procedure mentioned above. After 3 h, the rats were subjected to CT to confirm embolization. All CT examinations were performed as previously described (33) using a 16-slice multidetector row CT (Spuria, Hitachi Corporation, Japan). The scan parameters were as follows: 120 kV, 215 mA, 0.75 s/rotation, beam pitch 1.3125, collimation 1.25 × 16, slice thickness 1.25 mm. All of the images were recorded and analyzed using an image workstation (VINCENT, Fujifilm, Japan).

H&E staining was performed for histological analysis. In brief, all of the tissues were immersed in 4% paraformaldehyde for over 24 h. Each tissue sample was placed in a processing cassette, dehydrated through a serial alcohol gradient, and embedded in paraffin wax blocks. Next, the paraffin sections (7 μm) were dewaxed in xylene, rehydrated using decreasing concentrations of ethanol, and washed in deionized water. Then, the sections were subjected to H&E staining. Subsequently, the sections were dehydrated using increasing concentrations of ethanol and xylene and microscopically analyzed.

Immunohistochemical staining was performed on paraffin-embedded sections (6 μm thickness) for histological inflammatory analyses (T cells). Briefly, after dewaxing and dehydration, sections were preheated using heat-mediated antigen retrieval with sodium citrate buffer (pH 6) for 3 min and then cooled for 20 min. The sections were then incubated with anti-CD3 antibody (ab16669, Abcam) at 1/150 dilution for 60 min at room temperature and detected using a horseradish peroxidase–conjugated compact polymer system. 3,3′-Diaminobenzidine was used as the chromogen. Finally, the sections were counterstained with H&E and then enclosed for observation.

**Statistical Analysis.** All of the data were analyzed using a two-tailed unpaired Student's *t* test with unequal SDs. The mean difference between the control and experimental groups is shown as follows: ns, $P > 0.05$, $^{*}P < 0.05$, $^{**}P < 0.01$, $^{***}P < 0.001$.

**Data, Materials, and Software Availability.** All of the study data are included in the article and/or supporting information.

**ACKNOWLEDGMENTS.** This research was supported by JSPS KAKENHI grant nos. JP17H06144, JP17H06376, JP21K14676, and JPMJSP2119, and the Institute for Chemical Reaction Design and Discovery (WPI-ICReDD), which was established by the World Premier International Research Initiative (WPI), MEXT, Japan. The authors thank Mr. Yoshiyuki Saruwatari at Osaka Organic Chemistry for providing the chemicals.

Author affiliations: [a]Department of Neurosurgery, Faculty of Medicine and Graduate School of Medicine, Hokkaido University, Sapporo 060-8638, Japan; [b]Institute for Chemical Reaction Design and Discovery (WPI-ICReDD), Hokkaido University, Sapporo 001-0021, Japan; [c]Faculty of Advanced Life Science, Hokkaido University, Sapporo 001-0021, Japan; [d]Department of Forensic Medicine, Faculty of Medicine, Hokkaido University, Sapporo 060-8638, Japan; and [e]Center for Cause of Death Investigation, Faculty of Graduate School of Medicine, Hokkaido University, Sapporo 060-8638, Japan

Author contributions: H.F., T.O., T.N., and T.K. generated the concept; H.F., T.O., T.N., and T.K. designed research; Z.J., H.F., H.H., K.M., and A.T. performed research; Z.J. and H.F. performed in vitro and ex vivo experiments; Z.J. performed in vivo experiments; H.H., K.M., and A.T. performed CT scans; Z.J., H.F., T.O., J.P.G., and M.F. analyzed data; Z.J. and H.F. wrote the paper; and T.O., T.N., T.K., J.P.G., and M.F. provided comments on the manuscript.

1. C. J. Chen *et al.*, Brain arteriovenous malformations: A review of natural history, pathobiology, and interventions. *Neurology* **95**, 917–927 (2020).
2. G. Soulez, P. Gilbert, M. F. Giroux, J. N. Racicot, J. Dubois, Interventional management of arteriovenous malformations. *Tech. Vasc. Interv. Radiol.* **22**, 100633 (2019).
3. K. Schimmel *et al.*, Arteriovenous malformations-current understanding of the pathogenesis with implications for treatment. *Int. J. Mol. Sci.* **22**, 9037 (2021).
4. P. Pan *et al.*, Review of treatment and therapeutic targets in brain arteriovenous malformation. *J. Cereb. Blood Flow Metab.* **41**, 3141–3156 (2021).
5. J. Hu *et al.*, Advances in biomaterials and technologies for vascular embolization. *Adv. Mater.* **31**, e1901071 (2019).
6. H. Yang *et al.*, Injectable PEG/polyester thermogel: A new liquid embolization agent for temporary vascular interventional therapy. *Mater. Sci. Eng. C* **102**, 606–615 (2019).

7. G. Ko *et al.*, In vivo sol-gel reaction of tantalum alkoxide for endovascular embolization. *Adv. Healthc. Mater.* **11**, e2101908 (2022).
8. J. Lord, H. Britton, S. G. Spain, A. L. Lewis, Advancements in the development on new liquid embolic agents for use in therapeutic embolisation. *J. Mater. Chem. B Mater. Biol. Med.* **8**, 8207–8218 (2020).
9. L. Fan *et al.*, Injectable and radiopaque liquid metal/calcium alginate hydrogels for endovascular embolization and tumor embolotherapy. *Small* **16**, e1903421 (2020).
10. H. Oowaki *et al.*, Non-adhesive cyanoacrylate as an embolic material for endovascular neurosurgery. *Biomaterials* **21**, 1039–1046 (2000).
11. D. F. Vollherbst, R. Chapot, M. Bendszus, M. A. Möhlenbruch, Glue, onyx, squid or PHIL? Liquid embolic agents for the embolization of cerebral arteriovenous malformations and dural arteriovenous fistulas. *Clin. Neuroradiol.* **32**, 25–38 (2022).
12. N. Higashino *et al.*, Feasibility and safety of n-butyl cyanoacrylate-lipiodol-iopamidol as an alternative liquid embolic material. *Cardiovasc. Intervent. Radiol.* **44**, 482–488 (2021).
13. L. P. Mueller *et al.*, Neurotoxicity upon infusion of dimethylsulfoxide-cryopreserved peripheral blood stem cells in patients with and without pre-existing cerebral disease. *Eur. J. Haematol.* **78**, 527–531 (2007).
14. J. P. Jones, M. Sima, R. G. O'Hara, R. J. Stewart, Water-borne endovascular embolics inspired by the undersea adhesive of marine sandcastle worms. *Adv. Healthc. Mater.* **5**, 795–801 (2016).
15. A. Poursaid, M. M. Jensen, E. Huo, H. Ghandehari, Polymeric materials for embolic and chemoembolic applications. *J. Control. Release* **240**, 414–433 (2016).
16. S. Kim, K. W. Nowicki, B. A. Gross, W. R. Wagner, Injectable hydrogels for vascular embolization and cell delivery: The potential for advances in cerebral aneurysm treatment. *Biomaterials* **277**, 121109 (2021).
17. N. Schmitt *et al.*, Imaging artifacts of liquid embolic agents on conventional CT in an experimental in vitro model. *AJNR Am. J. Neuroradiol.* **42**, 126–131 (2021).
18. S. A. Smith, R. J. Travers, J. H. Morrissey, How it all starts: Initiation of the clotting cascade. *Crit. Rev. Biochem. Mol. Biol.* **50**, 326–336 (2015).
19. S. Walayat *et al.*, Role of albumin in cirrhosis: From a hospitalist's perspective. *J. Community Hosp. Intern. Med. Perspect.* **7**, 8–14 (2017).
20. J. N. Israelachvili, *Intermolecular and Surface Forces* (Academic Press, ed. revised 3, 2011), p. 710.
21. H. Fan *et al.*, Adjacent cationic-aromatic sequences yield strong electrostatic adhesion of hydrogels in seawater. *Nat. Commun.* **10**, 5127 (2019).
22. H. L. Fan, Y. R. Cai, J. P. Gong, Facile tuning of hydrogel properties by manipulating cationic-aromatic monomer sequences. *Sci. China Chem.* **64**, 1560–1568 (2021).
23. M. Kaibara, Rheology of blood coagulation. *Biorheology* **33**, 101–117 (1996).
24. M. Shahidi *et al.*, A comparative study between platelet-rich plasma and platelet-poor plasma effects on angiogenesis. *Med. Mol. Morphol.* **51**, 21–31 (2018).
25. V. Oöpik *et al.*, Effects of sodium citrate ingestion before exercise on endurance performance in well trained college runners. *Br. J. Sports Med.* **37**, 485–489 (2003).
26. H. Bruus, *Theoretical Microfluidics* (Oxford University Press) 2008).
27. R. K. Avery *et al.*, An injectable shear-thinning biomaterial for endovascular embolization. *Sci. Transl. Med.* **8**, 365ra156 (2016).
28. F. Cilurzo *et al.*, Injectability evaluation: An open issue. *AAPS PharmSciTech* **12**, 604–609 (2011).
29. A. Vo, M. Doumit, G. Rockwell, The biomechanics and optimization of the needle-syringe system for injecting triamcinolone acetonide into keloids. *J. Med. Eng.* **2016**, 5162394 (2016).
30. R. Siekmann, Basics and principles in the application of Onyx LD liquid embolic system in the endovascular treatment of cerebral arteriovenous malformations. *Interv. Neuroradiol.* **11** (suppl. 1), 131–140 (2005).
31. C. Senturk, Mechanical removal of migrated onyx due to microcatheter rupture during AVM embolization: A technical case report. *Cardiovasc. Intervent. Radiol.* **38**, 1654–1657 (2015).
32. A. K. Gaharwar *et al.*, Shear-thinning nanocomposite hydrogels for the treatment of hemorrhage. *ACS Nano* **8**, 9833–9842 (2014).
33. H. Hyodoh *et al.*, The infusion effect in postmortem lung CT. *Forensic Imaging* **20**, 200367 (2020).